The SAMI Galaxy Survey: Kinematics of Stars and Gas in Brightest Group Galaxies— The Role of Group Dynamics

Mojtaba Raouf[1] , Rory Smith[1] , Habib G. Khosroshahi[2], Jesse van de Sande[3,4] , Julia J. Bryant[3,4,5] , Luca Cortese[3,6] ,
S. Brough[3,7] , Scott M. Croom[3,4], Ho Seong Hwang[1] , Simon Driver[6] , Ángel R. López-Sánchez[3,8,9] , Jongwan Ko[1] ,
Jae-Woo Kim[1] , Jihye Shin[1] , Nicholas Scott[3,4], Joss Bland-Hawthorn[4] , Samuel N. Richards[10], Matt Owers[8,11] ,
J. S. Lawrence[12], and Iraklis S. Konstantopoulos[13]

[1] Korea Astronomy and Space Science Institute, 776 Daedeokdae-ro Yuseong-gu, Daejeon 305-348, Republic of Korea; mojtaba.raouf@gmail.com
[2] School of Astronomy, Institute for Research in Fundamental Sciences (IPM), Tehran, 19395-5746, Iran
[3] ARC Centre of Excellence for All Sky Astrophysics in 3 Dimensions (ASTRO 3D), Australia
[4] Sydney Institute for Astronomy (SIfA), School of Physics, University of Sydney, NSW 2006, Australia
[5] Australian Astronomical Optics, AAO-USydney, School of Physics, University of Sydney, NSW 2006, Australia
[6] International Centre for Radio Astronomy Research (ICRAR), The University of Western Australia, 35 Stirling Highway, Crawley, WA 6009, Australia
[7] School of Physics, University of New South Wales, NSW 2052, Australia
[8] Department of Physics and Astronomy, Macquarie University, NSW 2109, Australia
[9] Australian Astronomical Optics, Macquarie University, 105 Delhi Rd, North Ryde, NSW 2113, Australia
[10] SOFIA Science Center, USRA, NASA Ames Research Center, Building N232, M/S 232-12, P.O. Box 1, Moffett Field, CA 94035-0001, USA
[11] Astronomy, Astrophysics and Astrophotonics Research Centre, Macquarie University, Sydney, NSW 2109, Australia
[12] Australian Astronomical Optics—Macquarie, Macquarie University, NSW 2109, Australia
[13] Contact Energy, 29 Brandon Street, Wellington 6011, New Zealand

Abstract

We study the stellar and gas kinematics of the brightest group galaxies (BGGs) in dynamically relaxed and unrelaxed galaxy groups for a sample of 154 galaxies in the SAMI galaxy survey. We characterize the dynamical state of the groups using the luminosity gap between the two most luminous galaxies and the BGG offset from the luminosity centroid of the group. We find that the misalignment between the rotation axis of gas and stellar components is more frequent in the BGGs in unrelaxed groups, although with quite low statistical significance. Meanwhile, galaxies whose stellar dynamics would be classified as "regular rotators" based on their kinemetry are more common in relaxed groups. We confirm that this dependency on group dynamical state remains valid at fixed stellar mass and Sérsic index. The observed trend could potentially originate from a differing BGG accretion history in virialized and evolving groups. Among the halo relaxation probes, the group BGG offset appears to play a stronger role than the luminosity gap on the stellar kinematic differences of the BGGs. However, both the group BGG offset and luminosity gap appear to roughly equally drive the misalignment between the gas and stellar component of the BGGs in one direction. This study offers the first evidence that the dynamical state of galaxy groups may influence the BGG's stellar and gas kinematics, and we call for further studies using a larger sample with higher signal-to-noise.

Unified Astronomy Thesaurus concepts: Galaxy kinematics (602); Galaxy rotation (618); Galaxy evolution (594); Galaxy groups (597); Galaxy mergers (608); Galaxy dynamics (591)

1. Introduction

Galaxies are rarely found in isolation—they tend to aggregate together into small collections of galaxies known as galaxy groups, consisting of a few up to several hundred members, depending on the mass of the group. In most cases, the low-velocity dispersion of groups makes them ideal environments for efficient galaxy interactions and mergers. Furthermore, environmental mechanisms such as tidal stripping (Han et al. 2018), starvation (Larson et al. 1980), and ram pressure stripping (Gunn & Gott 1972; Park & Hwang 2009) may impact galaxy evolution, long before galaxies reach the denser environments of clusters (so-called "group pre-processing;" see Mihos (2004)). The impact of mergers on a galaxy may differ depending on the type of merger. Minor mergers are less disruptive but more frequent, while major mergers can significantly transform a galaxy's morphology and dynamics. The mergers may also be dry (i.e., the merger does not bring new gas) or wet (the secondary galaxy brings new gas), and this also impacts on the final formation result.

The impact of a merger on the gas kinematics is greater than on the stellar dynamics of galaxies (Barrera-Ballesteros et al. 2015). Simulations of galaxy mergers suggest timescales of ~2 Gyr for the gas disk to realign with the stellar component following the merger in the formation of massive early-type galaxies (van de Voort et al. 2015).

Bryant et al. (2019) used 618 galaxies with fitted gas and stellar position angle (hereafter: PA) from the Sydney-AAO Multi-object Integral field (SAMI) galaxy survey and found that ~45% of early-type galaxies and ~5% of late-type galaxies have a gas PA offset of more than 30° with respect to the stars. They found a stronger correlation of the gas–star misalignment with morphology compared to the stellar mass, color, or local environment of galaxies. Furthermore, Davis & Bureau (2016) showed that the gas–star misalignment in early-type galaxies could also originate from a continuous external

gas accretion, and thus major mergers are not the only possible origin. Jin et al. (2016) studied the fraction of gas–star misalignment in different stellar mass ranges and demonstrated that the fraction peaks at $10^{10.5}M_{\odot}$. Bassett et al. (2017) showed that the dust in the majority of early-type galaxies with an existing kinematical misalignment between the gas and stars, mostly has its origin in external dust brought in by the merger and is less likely to be produced internally by the AGB stars (see, e.g., Saremi et al. 2020).

Krajnović et al. (2011) classified galaxies by kinematic asymmetry to analyze the mean velocity map labeled as regular and nonregular rotators using a sample of 260 early-type galaxies in the ATLAS^{3D} survey. They reported that around 82% of galaxies are regular rotators, compared to just 17% nonregular rotators, where nonregular rotators are typically found in dense regions and are massive (e.g., Brough et al. 2017). The dynamical properties of early-type galaxies are related to a measure of their specific angular momentum, such that the merger remnant absorbs the orbital angular momentum of the merged galaxies in its internal dynamics (Lagos et al. 2015; van de Voort et al. 2015). Furthermore, using the projected angular momentum/spin and ellipticity, some studies show that the vast majority of early-type galaxies are actually fast rotating and have a regular stellar rotation (Emsellem et al. 2011; Cappellari 2016).

While the time difference between the peak of the brightest group galaxy (BGG) major merger in relaxed and unrelaxed groups is typically around ∼2 Gyr, most of the BGG last major mergers have occurred over the past 1 Gyr in unrelaxed groups (Raouf et al. 2018). This timescale for the last major merger of the BGG in unrelaxed group is below the relaxation timescale in which galaxy gas–star misalignment PA persists following an episode of reaccretion of cold gas (van de Voort et al. 2015) post merger.

Using the Galaxy And Mass Assembly (GAMA) galaxy survey, we showed that the BGGs of unrelaxed groups are significantly bluer in $NUV - r$ colors and tend to have higher stellar metallicity and star formation rates compared to BGGs of relaxed group at a given stellar mass (Raouf et al. 2019). Moreover, Khosroshahi et al. (2017) used the same sample of BGGs and found that the radio luminosity of the BGGs strongly depends on their dynamical state, such that the BGGs in dynamically unrelaxed groups are an order of magnitude more luminous in the radio than those with a similar stellar mass but residing in dynamically relaxed groups. They suggested that the presence of a high r-band magnitude gap between the two most luminous galaxies (luminosity gap) points to a scenario in which an earlier major merger could have triggered cold mode accretion, consistent with the associated 1.4 GHz AGN radio emission predicted by our semianalytical galaxy formation model (Radio-SAGE; Raouf et al. 2017, 2019). In our earlier study, using hydrodynamical simulations, we showed that the black hole accretion in BGGs of dynamically relaxed groups is lower, for a given stellar mass, than that in unrelaxed groups (Raouf et al. 2016). These pieces of evidence highlight clear differences in the observed properties of BGGs hosted by groups with different dynamical states. Here, we investigate the gas and star kinematics of BGGs to evaluate *the role of group dynamical states*.

We define the group dynamical state using a combination of two parameters, the luminosity centroid deviation of the BGG (i.e., the BGG offset) and the luminosity gap, which provide valuable information on the host halo formation history of BGGs (as demonstrated in cosmological simulations; see Raouf et al. (2014)). In this study, we determine whether the group halo formation history has any impact on the kinematic properties of the BGGs. We attempt to answer the above question by studying data from GAMA (Driver et al. 2011) and SAMI (Croom et al. 2012). Our relaxedness state indicators are best applied to statistically large samples of galaxies, rather than on a one-by-one basis, and these surveys provide us with sufficient numbers of galaxies (∼154) to make our study possible for the first time. Throughout this paper, we adopt $H_0 = 100h$ km s^{-1} Mpc^{-1} for the Hubble constant with $h = 0.7$.

2. Data and Sample Selection

The main sources of data for this study are the GAMA third data release (GAMA-DRIII; Driver et al. 2011; Baldry et al. 2018) and SAMI (Croom et al. 2012; Bryant et al. 2015) surveys.

GAMA is a multiwavelength spectroscopic data set covering an area of 180 deg^2 as described in Baldry et al. (2010), Robotham et al. (2010), Driver et al. (2011), and Hopkins et al. (2013). We use the third data release, GAMA-DRIII, group catalog generated for a spectroscopic component using a friends-of-friends (FoF) based grouping algorithm as described in Robotham et al. (2011). The group catalog contains 23,838 galaxy groups, which reduce to about 4000 galaxy groups (and about 19,000 group members) with a multiplicity of at least four spectroscopically confirmed members within the limit of our redshift range $0.02 < z < 0.22$ and in terms of having a complete set of groups in which the most and second-most luminous galaxies are detectable above the GAMA luminosity limit of $r = 19.8$ mag. The luminosity centroid,[14] stellar mass (Taylor et al. 2011), and ellipticity from an r-band Sérsic fit (Kelvin et al. 2012) of the group members are taken from the GAMA catalogs.

The SAMI instrument (Croom et al. 2012) is mounted on the 3.9 m Anglo-Australian Telescope (AAT) and fed into the AAOmega spectrograph (Sharp et al. 2006, 2015; Bland-Hawthorn et al. 2011; Allen et al. 2015; Green et al. 2018; Scott et al. 2018), which gives a median resolution of FWHM$_{blue} = 2.65$ Å from 3700–5700 Å and FWHM$_{red} = 1.61$ Å from 6300–7400 Å (van de Sande et al. 2017).

From all galaxies in the GAMA survey, there are ∼2200 galaxies that overlap with SAMI data within the redshift limit $z < 0.115$ from the G09, G12, and G15 regions (Driver et al. 2011). We focus on a sample that includes both stellar and gas kinematics in order to measure the PA offset. We include only those BGGs with $M_{star} \gtrsim 10^{10.6}M_{\odot}$ in order to have early-type galaxies in the group; see Figure 2 of Raouf et al. (2019) for the mass distributions of the main subsamples. Statistically, the final sample reduces to 154 galaxies, and we use the luminosity gap and BGG offset to categorize them into four different group subsamples (see Figure 1). In this study, we use kinematic properties from the internal data release Version 0.11.

The detailed description of the kinematic asymmetry, galactic spin, and misalignment angle measurements are given in the following subsections. Note that we use the Spearman correlation coefficient for the linear regression in our analysis.

---

[14] Defined as the center of light derived from the r-band luminosity of all the galaxies identified to be within the group (Robotham et al. 2011).
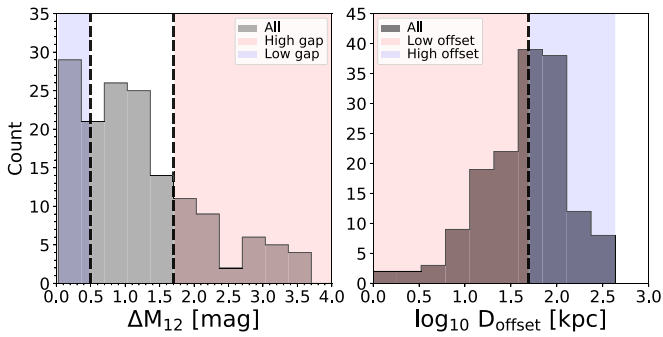
Figure 1. Histograms of the luminosity gap, ΔM_{12} (left), and BGG offset, D_{offset} (right), for all galaxies in the sample. Superimposed are limits for selecting high/low gap and low/high offset groups as shown by the shaded red/blue regions, respectively, separated by dashed lines.

2.1. Method to Estimate Kinematic Asymmetry

Similar to the method outlined in van de Sande et al. (2017), the kinematic asymmetry of the galaxy stellar velocity fields is determined by the amplitude of the Fourier harmonics on all velocity data that pass the velocity quality criteria measured using the kinemetry routine (Krajnović et al. 2006, 2011). The kinemetry routine determines a best-fitting amplitude for k_1, k_3, and k_5 for each ellipse. The first-order decomposition k_1 is equivalent to the rotational velocity, whereas the higher-order terms (k_3, k_5) describe the kinematic anomalies. In this study, the kinematic asymmetry[15] is defined as the luminosity-weighted average ratio of k_5/k_1 within one effective radius, R_e, determined by the flux in SAMI images. The uncertainty on k_5/k_1 for each measurement is estimated from Monte Carlo simulations. Note that we require a filling factor of 85% of the spaxels that pass the velocity quality criteria (for details, see van de Sande et al. (2017) and Scott et al. (2018)) within the aperture for producing R_e measurements. We now classify BGGs into regular (low k_5/k_1) and nonregular (high k_5/k_1) rotators, hosted by groups with differing dynamical states.

2.2. Spin of Galaxies

For each galaxy, the parameter λ_R is used as a proxy for the spin parameter. Following Emsellem et al. (2007), it is calculated using:

$$\lambda_R = \sum_i (F_i * R_i * |V_i|) \Big/ \sum_i (F_i * R_i * (V_i^2 + \sigma_i^2)^{1/2}), \quad (1)$$

where the subscript i refers to the ith spaxel within the ellipse, F_i is the flux of the ith spaxel, V_i is the stellar velocity in km s^{-1}, and σ_i is the velocity dispersion in km s^{-1}. For λ_R, R_i is the semimajor axis of the ellipse on which the spaxel i lies, where we use an ellipse at the effective radius, Re, in this study. We also estimate the ellipticity at the effective radius, ϵ_{Re}, from the best-fit MGE model (F. D'Eugenio 2021, in preparation).

2.3. Misalignment Angle

Stellar and gas kinematic measurements are derived for SAMI galaxies using the penalized pixel fitting code (pPXF; Cappellari & Emsellem 2004; Cappellari 2017) based on the method described in Krajnović et al. (2006). We use the FIT-

KINEMATIC-PA code to measure the PA of the 2D stellar/gas rotation (as described in van de Sande et al. (2017) and Fogarty et al. (2014)) on all spaxels that pass the quality cut for the velocity measurements, following the method described in Appendix C of Krajnović et al. (2006). The kinematic PA is measured assuming the center of the map is at (24.5, 24.5). The fit to the kinematic PA also includes measuring a 3σ uncertainty on that fit that can maximally be 90°. Because we provide a 1σ uncertainty in this catalog, the maximum error of the PAs is 30°. The kinematic PA is measured counter-clockwise, with 0° being north ($y = 0$) in the sky. Note that, for the 1σ errors, any PA with an uncertainty value close to 30° means the fit is not very reliable. However, this occurs in less than 5% of all the SAMI samples.

Misalignment angles for SAMI galaxies are defined as the difference between the kinematic PA of the gas (PA$_{GK}$) and the stars (PA$_{SK}$) when both velocities could be fitted with a reliable PA. We refer to these misalignment angles as the PA offset (δPA), and they always lie between 0° and 180°. Following other studies in the literature, (e.g., Lagos et al. 2015; Davis & Bureau 2016; Bryant et al. 2019), we assume that galaxies with a misalignment angle δPA $= |$PA$_{SK} -$ PA$_{GK}|$ of less than 30° are aligned (A). Otherwise, we refer to them as misaligned (MA) galaxies. If δPA is between 150° and 180°, we consider them as counter-rotating (CR) BGGs (extreme cases of MA galaxies). We also ran tests where we varied the critical angle required for a BGG to be considered misaligned from the standard value of 30°. In general, when we change the angle from 30° to 15°, the results agree within the errors and so they are not extremely sensitive to our exact choice of this critical angle.

The H$_\alpha$ emission line is used to measure the gas dynamics. The signal-to-noise ratio (S/N) is estimated for each galaxy individually based on the median value of the S/N for nonzero spaxels within R_e of a galaxy after removing the outlier spaxels ($\gtrsim 3\sigma$) using a σ-clipping approach. In this study, we labeled those galaxies with S/N > 4 and S/N < 4 as high (HSN) and low (LSN) S/N galaxies, respectively. We also did further cleaning of our sample by checking the trustworthiness of the H$_\alpha$ emission line maps by eye, in order to remove those few objects ($\lesssim 5\%$ of the sample) that survive that S/N cut yet we still cannot measure a reliable PA$_{GK}$ from.

2.4. Sample Selection

We focus on the BGGs ($M_* > 10^{10.6} M_\odot$) hosted by the groups with at least four members and whose halo mass peaks around $10^{13.25} - 10^{13.75} M_\odot$.[16] Our galaxy groups are separated into dynamically relaxed and unrelaxed subsamples using the following criteria:

Criterion I: Galaxy groups with a large luminosity gap between the BGG and the second-brightest group member, $\Delta M_{12} \geqslant 1.7$ ("high gap") in r-band within half the virial radius of the group. In addition, we also impose that the BGG is located within a radius of 50 kpc from the luminosity/stellar-mass centroid of the group ("low offset"). This criterion reduces our subsample to 35 galaxy groups, labeled as "relaxed" systems.

Criterion II: Galaxy groups with a small luminosity gap, $\Delta M_{12} \leqslant 0.5$ ("low gap") in r-band within half the virial radius of the group. We impose the BGG to be located outside a

---

[15] There is another definition of kinematic asymmetry, $(k_3 + k_5)/2k_1$ as described in Shapiro et al. (2008), which is consistent with the k_5/k_1 measurement of van de Sande et al. (2017).

[16] Groups with N < 4 spectroscopic members have a large uncertainty on the estimation of halo mass and other group parameters (Robotham et al. 2011).
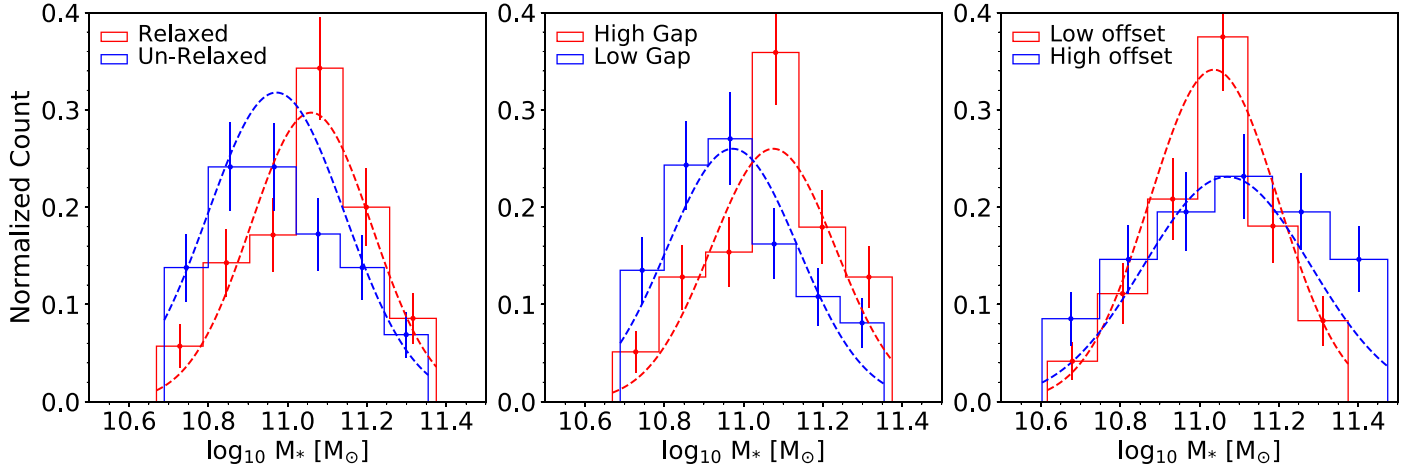
Figure 2. Distribution of stellar mass with Poisson errors for all subsamples considered in this study, including relaxed/unrelaxed, high/low gap, and low/high offset, as shown by red/blue color in each panel from left to right. Dashed lines show the Gaussian fit to each distribution.

Table 1
The Group Number Counts and Percentages with 1σ Binomial Confidence Interval Errors: Low S/N (LSN), Various Kinematic δPA (A, MA, and CR), Kinematic Asymmetry (NR, QR, and R), and Fast and Slow Rotators of BGGs Residing in Subsamples

Shape	High Gap	Low Gap	High Offset	Low Offset	Relaxed	Unrelaxed
Total Number	39	37	82	72	35	29
Alignment(A)	$38.5\% \pm 6.9\%$	$32.4\% \pm 6.6\%$	$29.3\% \pm 6.5\%$	$40.8\% \pm 5.4\%$	$40.0\% \pm 6.8\%$	$27.6\% \pm 5.9\%$
Misalignment(MA)	$20.5\% \pm 5.9\%$	$35.1\% \pm 6.7\%$	$28.0\% \pm 6.6\%$	$18.3\% \pm 6.7\%$	$20.0\% \pm 5.7\%$	$37.9\% \pm 6.5\%$
Counter-rotating(CR)	$10.3\% \pm 5.9\%$	$2.7\% \pm 6.7\%$	$6.1\% \pm 6.6\%$	$9.9\% \pm 6.7\%$	$11.4\% \pm 5.7\%$	$3.4\% \pm 6.5\%$
Low S/N(LSN)	$30.8\% \pm 6.6\%$	$29.7\% \pm 6.5\%$	$36.6\% \pm 5.0\%$	$31.0\% \pm 6.7\%$	$28.6\% \pm 6.3\%$	$31.0\% \pm 6.1\%$
Nonregular	$41.2\% \pm 6.9\%$	$40.0\% \pm 6.8\%$	$48.6\% \pm 4.9\%$	$37.5\% \pm 5.0\%$	$38.7\% \pm 7.2\%$	$44.4\% \pm 7.8\%$
Quasi-regular	$17.6\% \pm 5.5\%$	$25.7\% \pm 6.1\%$	$22.2\% \pm 4.1\%$	$23.4\% \pm 4.4\%$	$16.1\% \pm 5.6\%$	$25.9\% \pm 7.0\%$
Regular	$41.2\% \pm 6.9\%$	$34.3\% \pm 6.6\%$	$29.2\% \pm 4.5\%$	$39.1\% \pm 5.1\%$	$45.2\% \pm 7.3\%$	$29.6\% \pm 7.2\%$
Slow Rotator(EE+11)	$41.0\% \pm 6.5\%$	$29.7\% \pm 6.2\%$	$37.5\% \pm 4.7\%$	$36.6\% \pm 4.4\%$	$42.9\% \pm 6.9\%$	$34.5\% \pm 7.2\%$
Slow Rotator(MC+16)	$43.6\% \pm 6.5\%$	$29.7\% \pm 6.2\%$	$40.3\% \pm 4.8\%$	$37.8\% \pm 4.5\%$	$42.9\% \pm 6.9\%$	$31.0\% \pm 7.1\%$
Fast Rotator(EE+11)	$53.8\% \pm 6.6\%$	$54.1\% \pm 6.7\%$	$55.6\% \pm 4.9\%$	$56.1\% \pm 4.6\%$	$51.4\% \pm 6.9\%$	$48.3\% \pm 7.6\%$
Fast Rotator(MC+16)	$51.3\% \pm 6.6\%$	$54.1\% \pm 6.7\%$	$52.8\% \pm 4.9\%$	$54.9\% \pm 4.6\%$	$51.4\% \pm 6.9\%$	$51.7\% \pm 7.6\%$

radius of 50 kpc centered on the luminosity/stellar-mass centroid of the group ("high offset"). This criterion reduces our subsample to 29 galaxy groups labeled as "unrelaxed" systems.

This selection criterion leads us to identify groups with a similar halo mass but differing substructure (see Figure 6) and formation epoch (Raouf et al. 2014, 2016, 2018; Farhang et al. 2017; Zhoolideh Haghighi et al. 2020). Note that the small difference between the adopted $\Delta m_{12} = 1.7$ limit used for the selection of the relaxed and high gap groups and the one conventionally used in previous studies of optical fossil groups (Ponman et al. 1994; Jones et al. 2003), $\Delta m_{12} = 2.0$, is chosen to increase the number statistics of the relaxed and high gap subsamples (see Figure 1 left panel). We also use $\Delta M_{12} \leqslant 0.5$ as our definition of optical nonfossil groups, based on the simulation study of Dariush et al. (2010). We choose the offset criteria based on the distribution of offset values found in our semianalytic model (see Figure 3 in Raouf et al. 2014) where the BGG offset distribution of dynamically relaxed groups peaks at around ∼50–70 kpc. In this study, we use 50 kpc for the minimum offset criteria, in order to increase the statistics in the unrelaxed and high offset subsamples (see right panel of Figure 1). We also note that the measurements derived from the semi-analytical models are based on the average of three

projections along the three Cartesian coordinates of the simulation box, to allow them to be fairly compared with the observations. The normalized distributions of BGG stellar mass for each subsample are shown in Figure 2 (see Table 1 for the group number counts). The figure shows that our various subsamples (high/low gap, low/high offset, and relaxed/ unrelaxed groups) have a fairly similar range of stellar mass. We note that there is a small offset in the stellar mass distributions between the relaxed and unrelaxed subsamples, which actually contributes to strengthening our conclusions later (Section 3.2). In Figure 3, we also show the distribution of stellar mass versus halo mass for the sample of relaxed and unrelaxed groups. As can be seen, the small stellar mass difference mentioned earlier is more significant in low-mass halos. Note that the host halo mass distribution is quite similar for the various subsamples and does not influence our results significantly overall. To try to remove source confusion, all group BCGs are required to have at least a 10 kpc projected separation between the most luminous galaxies and other group members. In this way, less than 5% of the total sample has more than one galaxy in the SAMI field of view that could artificially affect the PA estimation. However, we also visually check the kinematic maps by eye, to confirm that our results are not affected in these few cases.
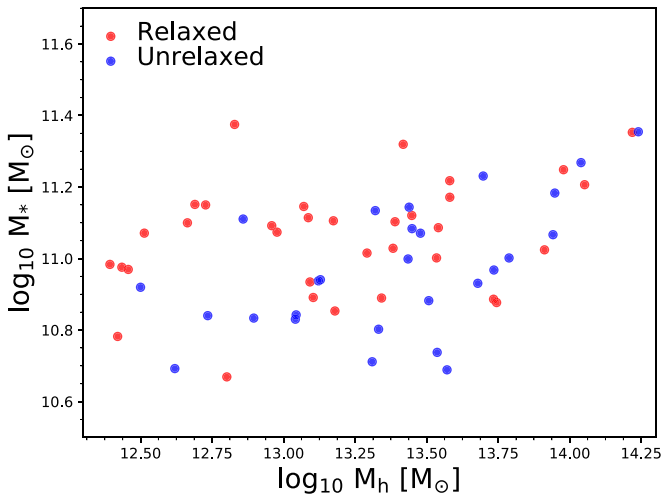
Figure 3. Distribution of stellar mass as a function of halo mass for the relaxed (red) and unrelaxed (blue) samples.

3. Results

Here, we compare the stellar regularities and rotational classification, then focus on the gas dynamics in order to compare the offset between the rotational axis of gas and stars in the BGGs of our subsamples. In order to get a feeling for the significance of the difference between the subsamples, we calculate one-sigma errors using the bootstrap method with iterations of $N = 1000$.

3.1. Stellar Dynamics in Our BGG Sample

3.1.1. Measurement of Regularity of BGG Rotation Using k_5/k_1

The top panels of Figure 4 show the distribution of the kinematic asymmetry (k_5/k_1) for BGGs in relaxed/unrelaxed (a_1), high/low gap (a_2), and low/high offset (a_3) groups. We define "regular rotation" (R) BGGs with $k_5/k_1 \leqslant 0.04$, "quasi-regular rotation" (QR) BGGs with $0.04 < k_5/k_1 < 0.08$, and "nonregular rotation" (NR) BGGs with $k_5/k_1 \geqslant 0.08$, following the approach of Krajnović et al. (2011) and similarly to that in van de Sande et al. (2017). Representative examples of stellar kinematic maps for an R(GAMA323558), a QR(GAMA272831), and an NR(GAMA209680) rotator BGG are presented in the figure. In the left panel of Figure 4(a_1), the BGGs in relaxed groups peak at k_5/k_1 values corresponding to those defined as regular rotators and decrease dramatically toward higher values of k_5/k_1. Considering the statistical error bars, the fraction of regular rotators for BGGs in unrelaxed groups is significantly lower at the 1σ level. We also conduct a Kolmogorov–Smirnov (KS) test of the difference in the distribution of relaxed and unrelaxed groups. Note that a resulting low KS statistic and/or smaller p-value indicates that the evidence for rejecting the null hypothesis of the same distribution is stronger. The resulting KS statistic is 0.17; however, the large p-value (0.68) indicates the difference between the distributions is of low significance (Table 2).

In the right panels (a_2), (a_3), we show the distribution of k_5/k_1 for the corresponding BGGs residing in low/high gap and high/low offset groups. While the BGG offset shows lower uncertainty compared to the luminosity gap, the BGGs in high offset groups have a higher fraction of nonregular rotators compare to the other subsamples. Once again, we conduct a KS test and find that, in the majority of cases, the BGGs in high offset groups tend to be nonregular, with a higher statistical difference (0.2) compared to the distribution of low offset groups (p-value = 0.07). This shows the higher significance of difference compared to the high/low gap groups (statistic = 0.14 , p-value = 0.8). However, we note that these histograms of the total distributions might not be expected to be as sensitive to the differences between the subsamples, because we do not control for any other parameter (e.g., mass). In general, around $\sim$45% of the relaxed groups consist of regular rotator BGGs, while the fraction is less than $\sim$29% for BGGs in unrelaxed systems. We also find the highest fraction of nonregular BGGs in high offset groups ($\sim$49%). All the above fractions, including their binomial errors, are reported in Table 1.

The bottom panels of Figure 4 show the fraction of regular BGGs at a given stellar mass for all subsamples, including errors based on the 1σ confidence intervals on the fractions, calculated using the bootstrap method. We try to get similar numbers in each stellar mass bin, as indicated with $N_{\rm gal}$ in the histogram panel on the upper x-axis (b_{11}). This leaves us with low $N_{\rm gal}$ in each bin, which is inevitable because we are sharing a small sample out over several bins. In the bottom left panel (b_1), the dashed line shows that the regular fraction decreases with stellar mass. The Spearman correlation coefficient for the linear regression between k_5/k_1 and stellar mass for all SAMI galaxies is $r_s = 0.33$, p-value = 0.0001. The correlation increases when we focus on BGGs in relaxed ($r_s = 0.56$, p-value = 0.002) and unrelaxed ($r_s = 0.45$, p-value = 0.02) groups. We also note that the unrelaxed groups are less regular in the upper panel (k_5/k_1 distributions), despite having slightly lower masses that could have resulted in a higher regular fraction. Hence, this further strengthens the differences seen in the top left panel, where we show the histogram of k_5/k_1.

The red line is generally above the blue line, except at the highest stellar masses, which shows that the unrelaxed groups have a less regular rotation at a fixed stellar mass, considering the 68% confidence interval errors (1σ). In addition, we also tried making a moving average plot of the regular fraction versus stellar mass (see the upper right inset figure in the bottom left panel (b_{12})). In this way, we ensure that each data point on the plot contains an equal number of (five) galaxies. As can be seen, the trend of regular BGG fraction in relaxed groups tends to be systematically offset above the BGGs in unrelaxed groups. Although the scatter is large, we believe this confirms the significance of the difference between the relaxed and unrelaxed subsamples. Overall, we see results similar to those found in the main panel, which confirms our conclusions that the relaxed groups tend to have BGGs whose stellar dynamics are systematically more regular.

The regular fractions of the corresponding low/high gap (panel (b_2)) and high/low offset (panel (b_3)) groups, as a function of stellar mass, are shown in the right panels. Both parameters have a similar trend in which the combination of the two parameters tend to complement each other in order to disentangle between the fraction of regular rotator BGGs in the relaxed and unrelaxed groups. The result shows that there is a difference in the fraction of regular rotator BGGs in the relaxed groups (i.e., those formed earlier) at a roughly 1σ confidence level compared to unrelaxed groups. It should be noted that the statistics in the individual points are inevitably quite poor, as we are spreading an already quite small sample over multiple stellar bins, although the significance is above 1σ in some individual points. When we split the sample by low and high offset, we get larger statistics in each data point, and the
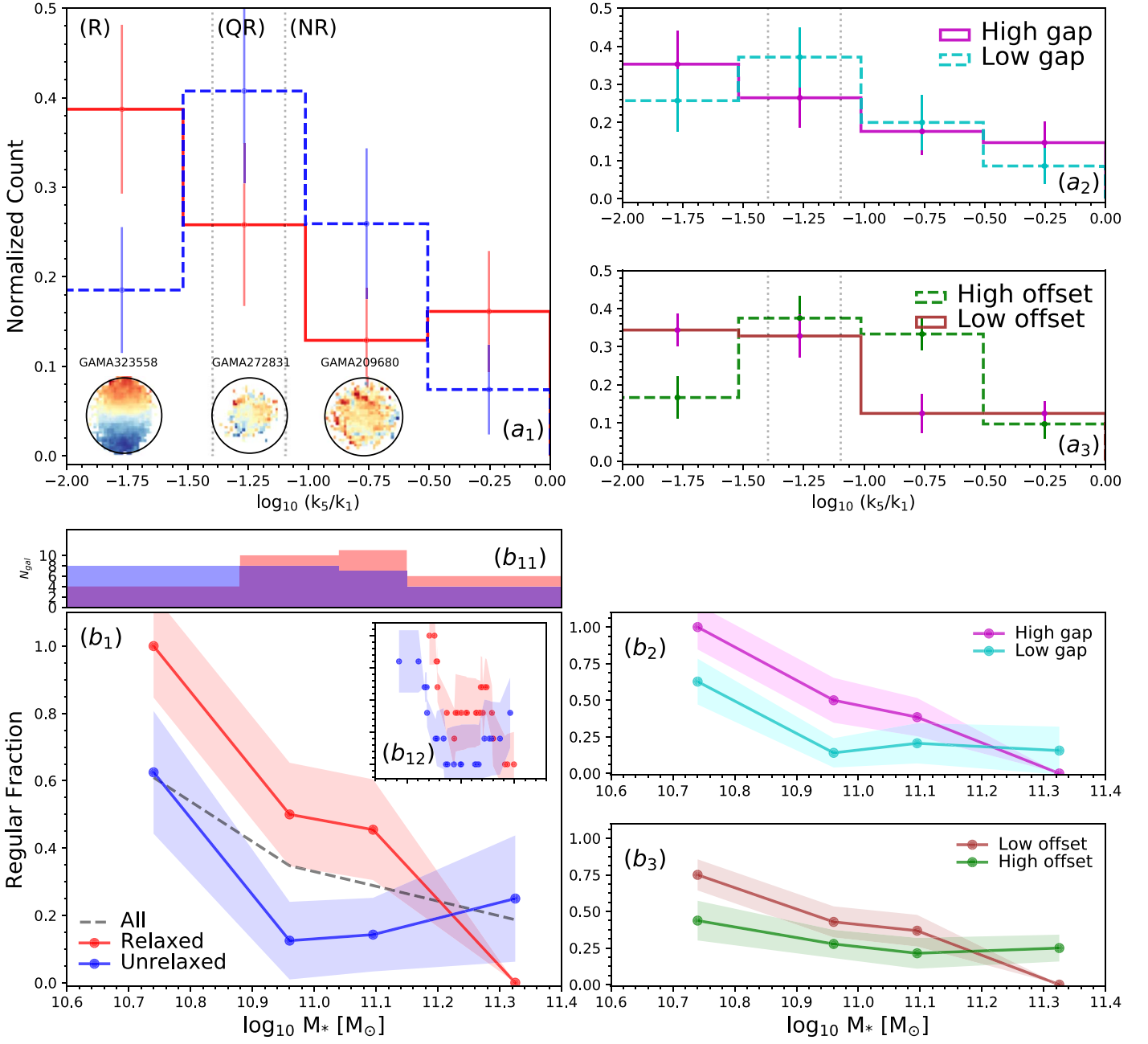
Figure 4. Top: distribution of the kinematic asymmetry (k_5/k_1) with standard deviation (σ) errors calculated by the bootstrap method for BGGs in relaxed (red) and unrelaxed (blue) group in the left panel (a_1), and high/low gap and low/high offset groups in the top (a_2) and bottom (a_3) right panels, respectively. The fraction of nonregular (NR) rotators ($k_5/k_1 > 0.08$), quasi-regular (QR) ($0.04 < k_5/k_1 < 0.08$), and regular (R) rotating ($k_5/k_1 \leqslant 0.04$) (dotted lines; van de Sande et al. 2017) are presented in Table 1 for the BGGs that reside in subsample groups. Representative stellar kinematic maps of BGGs defined as NR, QR, and R rotators are shown in the corresponding regions. Bottom: the fraction of regular BGGs as a function of stellar mass, separated by the subsample indicated in the legend (panels (b_1), (b_2), (b_3)). Dashed line shows the median trend for all BGGs in our sample. In each panel, the errors (color-shaded lines) are σ confidence intervals on the fractions calculated using the bootstrap method. In the histogram along the upper x-axis of the panel (b_{11}), we show the number of galaxies ($N_{\rm gal}$) in each stellar mass data point for the relaxed and unrelaxed samples. Inset figure in the left panel (b_{12}) shows the median fraction of regular rotation BGGs as a function of stellar mass using the moving average method where the axes range is the same as in the main plot.

Table 2
The KS Test Results (S: Statistic, P: *P*-value) for Comparing the Distribution of δPA and k_5/k_1 between the Different Subsamples of Groups

Subsample	δPA	k_5/k_1
Relaxed/unrelaxed	(S: 0.19, P: 0.78)	(S: 0.17, P: 0.68)
High/low gap	(S: 0.25, P: 0.33)	(S: 0.14, P: 0.82)
Low/high offset	(S: 0.11, P: 0.83)	(S: 0.20, P: 0.07)

significance of the difference between the subsamples seems to increase to slightly greater than 1σ.

3.1.2. The Spin Parameter of Our Sample

In Figure 5, we show the distribution of the spin parameter ($\lambda_{\rm Re}$) as a function of ellipticity ($\epsilon_{\rm Re}$) measured within the effective radius/ellipse as defined in van de Sande et al. (2017). This is the conventional diagram for separating galaxies into
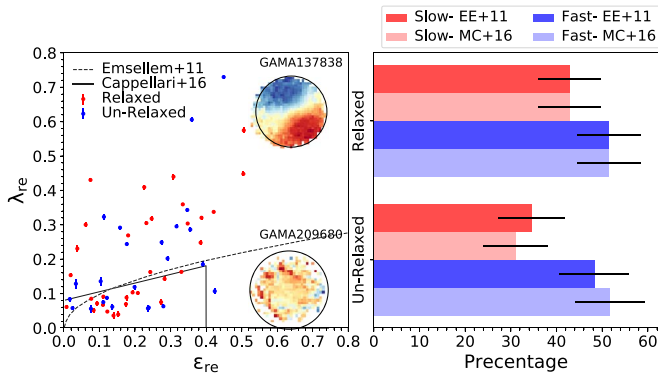
Figure 5. In the left panel, the spin parameter proxy within the effective radius ellipse, λ_{Re}, including measurement errors, is plotted as a function of galaxy ellipticity measured at the effective radius for BGGs in relaxed and unrelaxed groups. The various curves/lines separate galaxies into slow and fast rotators following the two separate schemes proposed in Emsellem et al. (2011, EE+11) and Cappellari (2016, MC+16). In the right panel, the fraction of slow and fast rotators is compared using horizontal bars with binomial errors for relaxed and unrelaxed groups. Representative examples of stellar kinematic maps are shown inside the figure for the fast (top) and slow (bottom) rotator BGGs.

slow- and fast-rotating subcategories (Emsellem et al. 2011; Cappellari 2016). By eye, it is not easy to see a clear difference between the relaxed and unrelaxed samples, but the horizontal bar plots in the right-hand panel reveal the statistics more clearly. The fraction of slow rotator BGGs is a bit higher (∼10%) in the relaxed system compared to the unrelaxed groups, while both samples have the same fraction of fast rotators BGGs as expected for the most early-type galaxies (van de Sande et al. 2017). A representative stellar kinematic map for fast (GAMA209680) and slow (GAMA137838) rotator BGGs is shown in this figure. In general, over 50% of our subsamples are fast-rotator BGGs, with the highest fraction for BGGs in low offset groups (∼55%). *We find that the BGGs of unrelaxed groups frequently rotate faster.* However, this result is of low significance due to low number statistics.

3.2. Kinematic Misalignment between the Gas and Stellar Dynamics

To measure the kinematic misalignment between the gas and stellar dynamics, we need to be able to trust both the stellar and gas dynamics individually to measure the difference in their PA. However, in practice, it is normally the gas that is the limiting factor, hence it was necessary to do some additional cleaning of the samples. We removed all objects whose gas PA maps were measured to be too LSN. This was accomplished in two steps. First, we removed all objects whose S/N criteria < 4 (LSN objects), and then we did some additional cleaning by eye (as described in Section 2.3). Concerning any bias in the population that can be the LSN galaxies compare to our full sample, we find the fraction of LSN galaxies is similar between relaxed and unrelaxed groups.

Figure 6 shows the $\Delta M_{12} - D_{offset}$ map with symbols that show the stellar kinematic of each individual galaxy in our sample. Representative examples of an aligned (A), misaligned (MA), and counter-rotating (CR) galaxy are shown for the gas and stellar velocity map and photometric postage stamp (see the Appendix for the full sample of relaxed and unrelaxed galaxies, respectively). The statistical percentage of A, MA, CR, and LSN for BGGs residing in relaxed and unrelaxed

groups are shown in the pie charts. Note that CR is an extreme subcategory of MA but with very low statistics in our sample, so here we merely report the percentages without using them as part of our main conclusion. The substructure of an ideal relaxed and unrelaxed group is shown in the corresponding box, with density contours extracted from the semi-analytic model (Radio-SAGE; Raouf et al. 2017).

In general, regarding the blue and red regions of galaxies in the map of $\Delta M_{12} - D_{offset}$, galaxies in the relaxed groups tend to be more aligned by over 40% and generally higher than the fraction of total misaligned BGGs including MA (∼20%) and CR (∼11.4%). Around ∼29% of galaxies in the relaxed group are LSN BGGs. On the other hand, almost ∼41% of the BGG in the unrelaxed group are misaligned (MA + CR). Such groups have ∼27.6% aligned and ∼31% LSN BGGs, with a ~3.4% fraction of CR galaxies. The percentage of other subsamples, including their binomial errors, are reported in Table 1. As might be expected, most of the LSN BGGs in our sample have uncertain δPA. We find that the removal of these objects has a similar impact on both the relaxed and unrelaxed groups.

Furthermore, the top left panel of Figure 7(a_1) shows the distribution of the kinematic misalignment angles of gas and stellar velocity map for BGGs in relaxed versus unrelaxed groups. Both relaxed and unrelaxed group have a peak in the aligned region (<30°), but with a more significant peak in the relaxed groups with respect to the unrelaxed groups. We conduct a KS test of the difference in the distributions of relaxed and unrelaxed groups and get a KS statistics of ∼0.2, with a large p-value (0.78), which indicates the low significance of the difference in their distribution (Table 2). On the right, we show the same plot but for high/low gap and low/high offset groups. While the shapes of the histograms are quite similar overall, a KS test reveals that the statistical difference between high/low gap groups is equal to 0.25, which seems slightly larger and more significant (p-value = 0.3) than in the low/high offset groups (statistic = 0.1, p-value = 0.8). This suggests that the luminosity gap is slightly more important for determining the amount of misalignment than the offset parameter. However, as we will show, it is important to take into account other parameters, such as the stellar mass and Sérsic index.

So far, overall, the difference in the gas–star δPA BGGs residing in groups with different dynamical states (and such different formation histories) has not been very significant. However, this is partly because we have combined all the galaxies in each subsample, regardless of their stellar mass or morphological shape. So now, in the middle/bottom panel of Figure 7(b_1/c_1), we show the fraction of misaligned BGGs at a given stellar mass/Sérsic index for the same subsamples (relaxed versus unrelaxed). Errors in the fractions are 1σ confidence intervals, calculated using the bootstrap method. Given the small sample size, there is no fully robust manner to calculate the errors. Therefore, we also try calculating our errors using the binomial confidence levels, separately. Both methods of measuring the errors give similar results, which gives us additional confidence in the significance of the differences that we quote. Note that the BGGs of unrelaxed groups are slightly lower mass in the middle left panel (b_1), which actually strengthens the significance of the difference seen in the first panel (i.e., the δPA distributions).
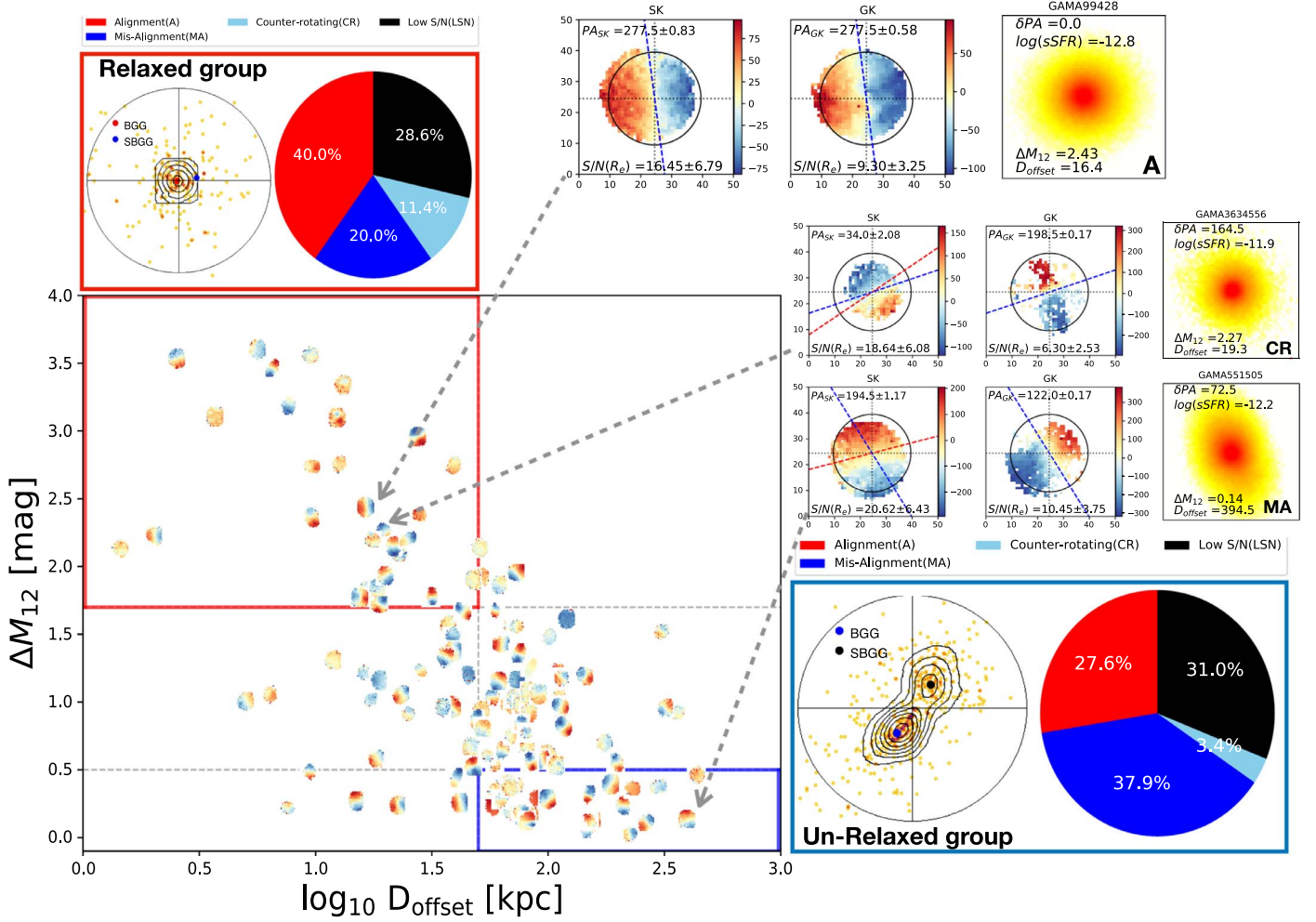
Figure 6. Map of luminosity gap, ΔM_{12}, as a function of BGG luminosity offset, D_{offset} symbolized by the BGGs stellar kinematic. Red and blue bordered squares highlight the limits of the regions inhabited by the relaxed and unrelaxed groups, respectively. Pie chart shows the fraction of aligned (A: red), misaligned (MA: blue), and counter-rotating (CR: sky blue) BGGs, as well as BGGs where there is too much uncertainty in their misalignment PA to classify them, due to low signal-to-noise (LSN: black) in the H_α velocity maps, within the effective radius (Re). Besides the pie charts, we present a representative example of a member of the relaxed and unrelaxed group, as found in the semi-analytic model from Raouf et al. (2017). The location of the brightest group galaxies (BGGs) and the second-brightest group galaxies (SBGGs) are highlighted with a filled circle symbol for each group. In the upper right panels, we provide representative examples of the stellar kinematics (SK), gas kinematics (GK) velocity map, and a postage stamp in r-band from the GAMA Panchromatic Swarp Imager (PSI), for a BGG in the relaxed and unrelaxed group. The major axes of rotation are shown by red and blue dashed lines in the SK and GK kinematic maps, respectively, along with the median signal to noise (S/N) in Re with STD error. Each kinematic map inside the panels has a $15''$ side length, and the SAMI bundle size is shown by the circle. In the r-band optical postage stamp (right panels), we also show the δPA, sSFR, ΔM_{12}, and D_{offset}.

In general, the gas–star kinematic misalignment angle has a stronger dependence on the Sérsic index in comparison to the stellar mass, as shown by comparing the Spearman coefficient correlation for linear regression (r_s) and the p-value for the entire sample (M_{star}: $r_s = 0.26$, p-value $= 0.005$; n_{Sersic}: $r_s = 0.38$, p-value $= 0.00005$). This is the same result as was found in Bryant et al. (2019), although the sample selection is very different in their study.

In the middle panel, along the upper x-axis (panel (b_{11})), we plot a histogram of the number of galaxies in each data point; this leaves us with low N_{gal} in each bin, which is inevitable because we are sharing a small sample out over several bins. Note that we choose the bins in a manner intended to get similar numbers in each data point, and the error bars are clearly larger when there are less galaxies in a data point. In the panel below the histogram (b_1), we show that, at a given stellar mass, the misaligned fraction of BGGs is higher for unrelaxed groups. The fraction for relaxed systems is consistently below the unrelaxed sample across the plot. However the significance

of the difference is weak for some points, perhaps due to the low statistics in each stellar mass bins. Note that we lose around 30% of the BGGs in the sample that do not have sufficient S/N to measure the gas dynamics position angle. The dashed line (panel (b_1)) shows that the misaligned fraction is greater in more massive galaxies. Despite the fact that our unrelaxed sample has slightly less massive galaxies (Figure 2), we still see that the unrelaxed groups have more misalignment in the upper left panel (b_1). This further strengthens the results seen in the distribution of galaxies, as the stellar mass difference could be partially canceling out the true difference. This also provides a motivation to split the sample by stellar mass. The corresponding low/high gap and high/low offset groups misaligned fraction as a function of stellar mass are shown in the center right panels ((b_2), (b_3)). These results show that the low gap groups tend to have a higher misaligned fraction relative to the high gap systems. The KS test results confirm that there is a greater statistical difference and significance between low/high gap groups than in the low/
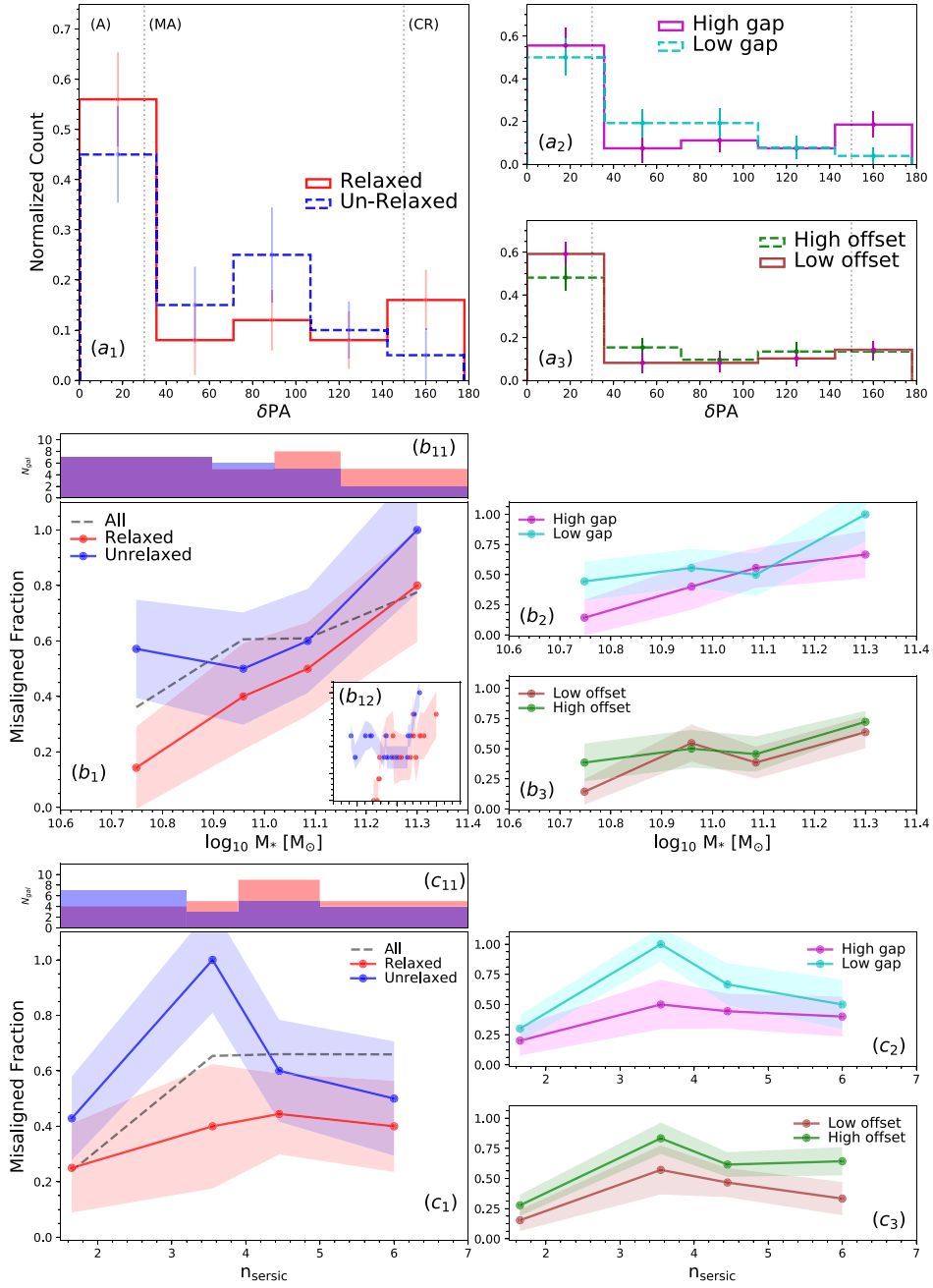
Figure 7. Top: distribution of the star–gas misalignment PA, δPA, for BGGs for relaxed/unrelaxed (panel (a_1)), high/low gap (top right panel (a_2)), and low/high offset (bottom right panel (a_3)) groups. Errors are standard deviation (1σ) errors calculated using the bootstrap method. Vertical dotted lines show δPA of $30°$ and $150°$ that we used for discriminating between alignment/misalignment (A/MA) and contour rotating (CR) BGGs, respectively. Middle: fraction of misaligned δPA as a function of stellar mass for BGGs, separated into the subsamples (b_1, b_2, b_3) given in the legend. Dashed lines show the median trend for all BGGs in our sample. In each panel, the errors (color-shaded lines) are 1σ confidence intervals on the fractions calculated using the bootstrap method. Along the upper x-axis of the panel (b_{11}), we show the stellar mass distribution of relaxed and unrelaxed in the bins (N_{gal}) in order to present the statistics in each data point. Inset figure in the left panel (b_{12}) shows the median fraction of misaligned δPA BGGs as a function of stellar mass using the moving average method with standard deviation error, where the axes range is the same as in the main panel. Bottom: Fraction of misaligned δPA as a function of BGGs Sérsic index (c_1, c_2, c_3), $n_{\rm Sersic}$, with the same description as given in the middle panel.

high offset groups (see Table 2). The subsamples have better number statistics for high/low offset groups, which leads to lower uncertainty with a more-or-less similar fraction of misaligned BGGs. As with the regular fraction, we also conducted a moving average test of misalignment fraction versus stellar mass (see inset figure in the middle left panel (b_{12})). This ensures that each data point contains an equal number of (five) galaxies. It can be seen that the trend of misaligned BGG fractions in unrelaxed groups tends to be

systematically above the BGG in relaxed, even though the scatter is large. Once again, we obtain similar results overall. These results are consistent with our conclusions regarding the impact of the group dynamical state on the misalignment of gaseous and stellar components, and they also confirm the significance of the differences between relaxed and unrelaxed groups seen in Figure 7. In summary, at a given stellar mass, a small but statistically significant difference has been shown for the BGGs hosted by groups with different dynamical states. In
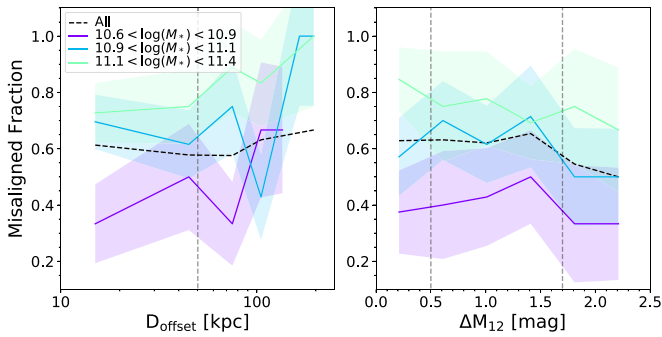
Figure 8. Fraction of misaligned gas–star PA for BGGs residing in groups with a varying luminosity gap, ΔM_{12} (right), and BGG offset, D_{offset} (left). Colored lines show the trend for three stellar mass bins. Black dashed lines show the median trend for all BGGs in our sample. Errors (color-shaded lines) are 1σ confidence intervals on the fractions calculated by the bootstrap method. Gray vertical dashed lines in each panel show the selection for low/high offset and high/low gap groups.

turn, their dynamical state is linked to the formation epoch, as shown in our earlier study using cosmological simulations (Raouf et al. 2016).

In the bottom panel of Figure 7(c_1), we repeat this process— but this time plotting against the Sérsic index, n_{Sersic} instead of the stellar mass. Again, we see that there is a higher fraction of misaligned BGGs in the unrelaxed groups compared to the relaxed systems.

Furthermore, the corresponding low/high gap (panel (c_2)) and high/low offset (panel (c_3)) groups show similar differences in misalignment fraction as a function of Sérsic index, as shown in the bottom right panels, again verifying the role of dynamical state on the BGG gas–star δPA independent of Sérsic index. Also, thanks to the higher number statistics of BGGs in the low and high offset groups (~2 times bigger than other subsamples), we see a slight increase in the significance of the difference between them, compared to the other subsamples. In other words, the late-formed systems (unrelaxed systems) tend to have a higher fraction of misaligned BGGs at fixed Sérsic indices.

In summary, for Figure 7, it is clear that the difference between the relaxed and unrelaxed groups is marginal in the distribution of δPA. However, when we split by stellar mass and Sérsic index, we find there are consistent offsets across most of the data points in the BGGs of relaxed and unrelaxed systems. The same offsets are also seen for the BGG offset and luminosity gap distribution, where the sample size is increased by a factor of ~2. The BGG offset and luminosity gap seem to cause roughly equally offsets for a fixed galaxy stellar mass or Sérsic index. Although each individual offset is of quite low significance, it is the combination of these results that gives us more confidence in our overall conclusions. However, we must note that *future larger samples will be crucial to enhance the significance of our result*.

Finally, in Figure 8, we show the fraction of BGGs that have misaligned gas–star PAs, hosted by the groups with different luminosity gap and BGG offset. The trends show three different stellar mass bins with roughly the same number of BGGs. All ΔM_{12} and D_{offset} bins include reasonable number statistics ($N > 3$), except for the very high gap and offset groups; the statistics are poor in those groups, as evident from the larger errors in those bins. Errors are given by the 1σ confidence intervals on the fractions, calculated using the bootstrap method. As can be seen, a higher fraction of

misaligned BGGs belongs to the stellar mass range over $10^{11.1} M_\odot$ (as already shown by the dashed line in Figure 7). The misaligned fraction overall tends to increase with BGG offset but slightly decreases with increasing luminosity gap. We note that, although both the gap and offset trend are quite noisy, they both have a slight trend in one direction.

4. Discussion and Conclusion

The focus of this study is the connection between the dynamical state of groups and the stellar and gas dynamics of BGGs using a sample of galaxy groups from the GAMA galaxy survey, where the internal kinematic properties of the BGG are measured in the SAMI survey. Our BGGs all have stellar masses over $10^{10.6} M_\odot$ with a similar host halo mass distribution. This choice of mass cut causes them to typically be early-type.

To probe the dynamical state of the group halo, we use a combination of two independent optical indicators: the luminosity gap between the two brightest galaxies, ΔM_{12} (within half a virial radius of the group), and the offset between the position of the BGG and group's luminosity weighted center, D_{offset}. Cosmological simulations show that such a selection indirectly leads us to identify BGGs with different merger histories (and different amounts of time since their last major merger; e.g., see Figure 2 in Raouf et al. (2018)).

For the measurement of the internal kinematics of the BGGs, in the stellar component, we use a Fourier analysis on the regularity of the rotation field (k_5/k_1 parameters; see Krajnović et al. (2008)), and also consider their location in the spin-ellipticity plane (e.g., Emsellem et al. 2011; Cappellari 2016). For the gas kinematics, we measure the position angle of rotation in their Hα emission map and compare it with the position angle from their stellar dynamics map (similar to that in Bryant et al. (2019)). The difference between these two position angles is known as the misalignment angle.

We demonstrate that there is a small but statistically significant difference (at the 1σ level) in the gas–star kinematics misalignment position angle (δPA), and separately, the regularity of the stellar rotation of BGGs, when comparing groups with differing dynamical states of relaxedness. We also present the results as a function of stellar mass and Sérsic index (in particular for δPA). We find a stronger correlation between gas–star misalignment and Sérsic index than with stellar mass, in agreement with Bryant et al. (2019).

The main results are as follows.

1. We find that the BGGs in unrelaxed groups tend to have stellar kinematics with less regular rotation fields than those in relaxed groups. The statistical significance is low (of order 1σ), perhaps in part due to poor statistics. When we split the sample into high/low offset and high/low luminosity gap, the results remain intact, and the larger samples give improved statistical significance.

2. Placing our sample in the spin parameter–ellipticity plane, we find that more than 50% of our sample of BGGs have a stellar component that is considered a fast rotator. There is a slightly higher fraction ($\gtrsim$10%) of slow rotators in relaxed groups with a low significance compared to the unrelaxed group. Thus, there is a weak indication that relaxed groups are more likely to host slow rotator BGGs (perhaps due to a slightly higher fraction of massive BGGs in relaxed groups).

3. Now considering the internal gas kinematics as well, we show that the BGGs in unrelaxed groups tend to have higher δPA compared to relaxed groups. Note that there is a possible trend between the groups' dynamics and the kinematics of BGGs, but that the result is not significant, considering the errors calculated using the bootstrap method.

4. Splitting the sample by stellar mass or Sérsic index, we find a clear correlation with δPA. We consistently find a higher fraction of misaligned BGGs hosted in unrelaxed groups. On one hand, given the small sample size, the statistical significance is low. On the other hand, when we split the sample into high/low offset and high/low luminosity gap subsamples, our statistics are improved slightly (by a factor of 2) and we see a consistent dependency on the dynamical state of the group, but now with greater significance.

5. In general, the luminosity gap and offset parameters seem to contribute roughly equally to our ability to differentiate relaxed and unrelaxed groups, within the range of parameters we consider in this study.

Although the statistical significance of any individual result is quite weak (perhaps due to our small sample size), they are all consistent with each other in terms of their dependency on the relaxation state of their group, which gives us added confidence that there is a true dependency. We note that, although our sample size is somewhat limited (64 galaxies in total from 154 galaxies), it is still the largest sample that could be collected from currently available surveys. The only way to fully confirm our results with greater significance would involve gathering a significantly larger sample.

We suggest that it takes time for galaxies to become regular rotators and/or for their gas and stars PA to align, and that the timescale for realignment is similar to the time it takes for a group to become dynamically relaxed. Recently, it has been shown that the relaxation timescale strongly depends on the mass assembly history of the host halo (Zhoolideh Haghighi et al. 2020). On the other hand, Raouf et al. (2018) showed that there is a 2 Gyr difference in the timescale of mass assembly history (on average) of the BGG in relaxed and unrelaxed groups. Furthermore, they showed that the time since the last major merger is statistically lower (typically in the last gigayear) for BGGs in unrelaxed groups compared to BGG in relaxed groups. Simulation studies of the formation of massive early-type galaxies suggest that the relaxation timescale (Lake & Norman 1983) for dynamical settling of the gaseous component into the stellar discs (gas–star realignment) after the merger is around 2 Gyr, depending on the extension of gas accretion (van de Voort et al. 2015). On this foundation, we claim that the group dynamical state leaves a traceable impact on the internal kinematics of both the stars and ionized gas in BGGs.

The emerging picture from this study is consistent with a number of previous studies that have focused on other aspects of the halo impact on the BGGs. For example, previous observations found that relaxed groups tend to have experienced gas-rich galaxy mergers (Khosroshahi et al. 2006; Brough et al. 2006a, 2006b) in their evolutionary history, compared to BGGs in unrelaxed systems but with equal stellar mass. In our recent studies, we showed that the luminosity gap parameter plays an important role in differences between the BGG stellar population properties such as metallicity, star

formation rate, dust, and NUV − r color (Raouf et al. 2019). We found that BGGs in relaxed groups typically have an earlier peak in their merger rate, ∼2 Gyr, and had not suffered a recent major merger (<1 Gyr Raouf et al. 2018). Generally speaking, the BGGs in relaxed groups have a lack of recent major mergers, and the more frequent misalignment of gas rotation with respect to their stars in the BGGs of unrelaxed groups could be the result of new gas externally accreted through their more recent last (major) mergers. As mentioned earlier, galaxies in denser environments show less regularity than those in less dense environments (Krajnović et al. 2011; Lee et al. 2018). Indeed, our result pushes the existing results to a new level by moving beyond studying the role of the local density on stellar kinematic to also considering the role of the group dynamics.

This paper suggests that the accreted gas, following a galaxy merger, would settle (i.e., the gas would relax) in such a way that its rotation axis is aligned with that of the stellar component (co-rotating or counter-rotating) when the timescale is equal to or shorter than the time since the BGG's last major merger; otherwise, the gas rotation axis would deviate from that of the stars. This is more likely if the major merger occurred in an earlier epoch during the evolution of the BGGs, as there will be more time available for the gas to settle in and around the stellar component. Therefore, it is conceivable (but with very low statistical significance, i.e., around 10% in this work) to find more counter-rotating and aligned BGGs for the groups with an earlier last major merger (e.g., BGGs in relaxed systems in this study). In the formation of an unrelaxed group, the time between the mergers is short enough that the gas is still misaligned from the last merger, while the group is still classified as unrelaxed due to its dense core. In such an environment, continuous accretion of gas (as a result of more frequent mergers, compared to the relaxed groups) leaves no time for gas to align with the stellar component.

Note that the fraction of new accreted gas and to the preexisting gas is also expected to be important for the overall gas relaxation timescale. An existing gas disk would relax much more quickly after a merger unless it was very massive and thus the gas richness might have an impact on the gas settling timescale (e.g., Lagos et al. (2015), Khim et al. (2020a, 2020b) for early-type galaxies). We also find unrelaxed groups with aligned, and relaxed groups with misaligned BGGs. One possibility is that some of our low Sérsic index objects might have contained gas prior to the merger, which could be consistent with the fact that we clearly see a higher aligned fraction for those objects. Another possibility is the fact that our optically measurement of the group dynamical state is not expected to be 100% correct on a one-to-one basis.

Our future study will focus on the source of external accretion, cooling the halo, and stripping or distortion of gas due to group processes by considering the location of galaxies in the cosmic web.

The SAMI Galaxy Survey is based on observations made at the Anglo-Australian Telescope. The Sydney-AAO Multiobject Integral field spectrograph (SAMI) was developed jointly by the University of Sydney and the Australian Astronomical Observatory. For the masses, redshift, and the rest: GAMA is a joint European-Australasian project based around a spectroscopic campaign using the Anglo-Australian Telescope. The GAMA input catalog is based on data taken

Appendix
Smoothing Map for Gas PA

To create the smoothed maps of the Hα emission maps that are visible in Figure 6, we use a convolution function with Gaussian kernel and integrated mode. In this way, we try to replace bad spaxels with values interpolated by neighbors (see Figures 9–12). We note that the smoothed maps are not used for measuring the gas PA. These smoothed maps are only used in combination with the original maps to aid us in evaluating by eye whether objects that survive our S/N cut are reliable for measuring the kinematic PA (Section 2.3). In each gas velocity map (GK), we only consider the spaxels with Hα S/N ratios less than 3 and velocity errors of over 30 km s^{-1}.
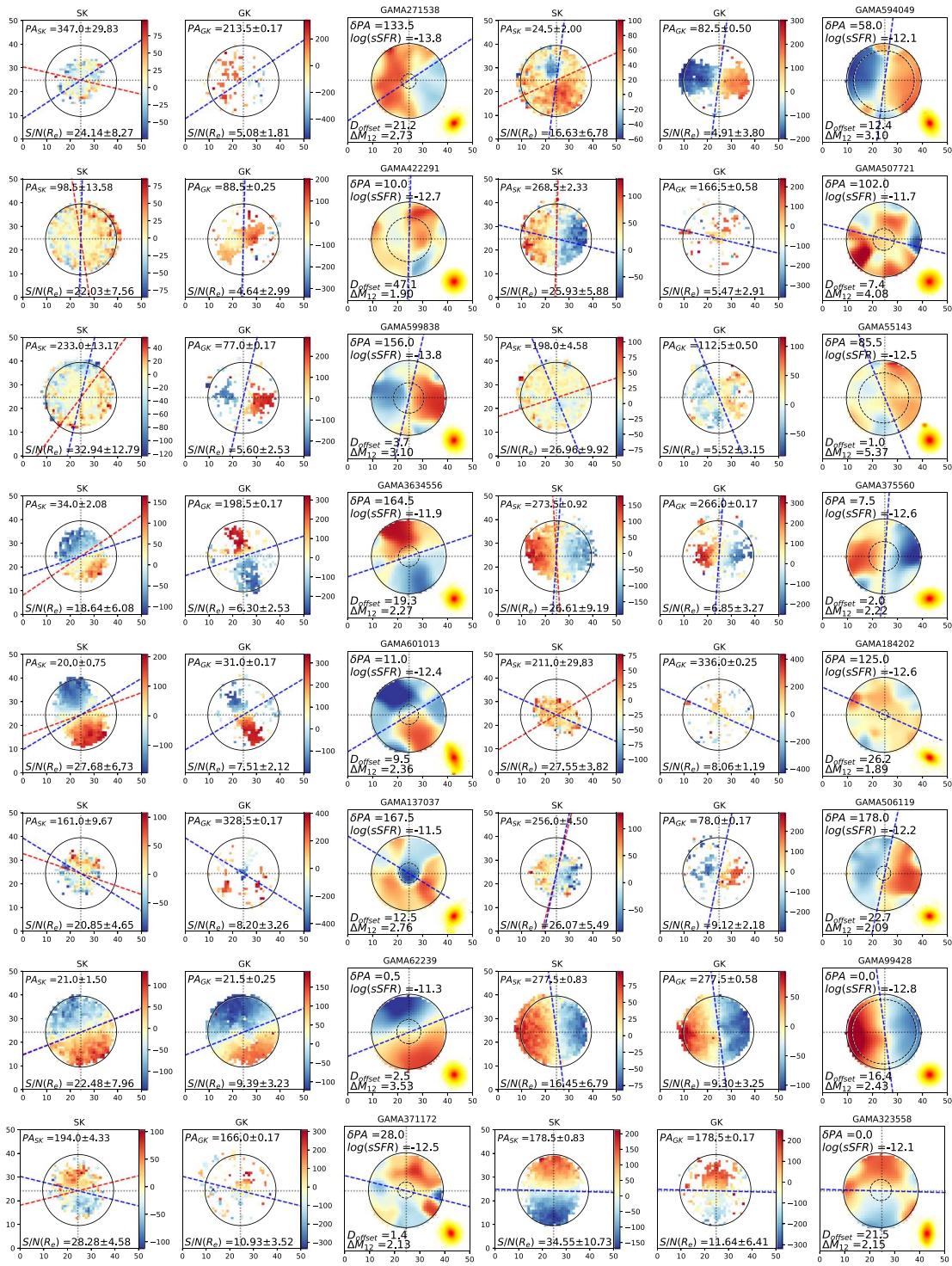
Figure 9. (left) Stellar kinematics (SK), and (center) Hα gas kinematics (GK) velocity maps. There are two galaxies per row. Labels indicate the PA with error and S/N within one effective radius. Circle indicates the 15″ size of the SAMI hexabundle. (right) Smoothed map of the GK, including labels with the GAMA ID, δPA, sSFR, and the group magnitude gap and BGG offset. Dashed circle indicates the effective radius (Re). Bottom right corner shows an inset image of a postage stamp in r-band from the GAMA Panchromatic Swarp Imager (PSI) with 20″ side length (note that inset image is on a very different scale from the SAMI images). Red and blue dashed lines show the major axes of rotation for stellar and gas kinematics, respectively.
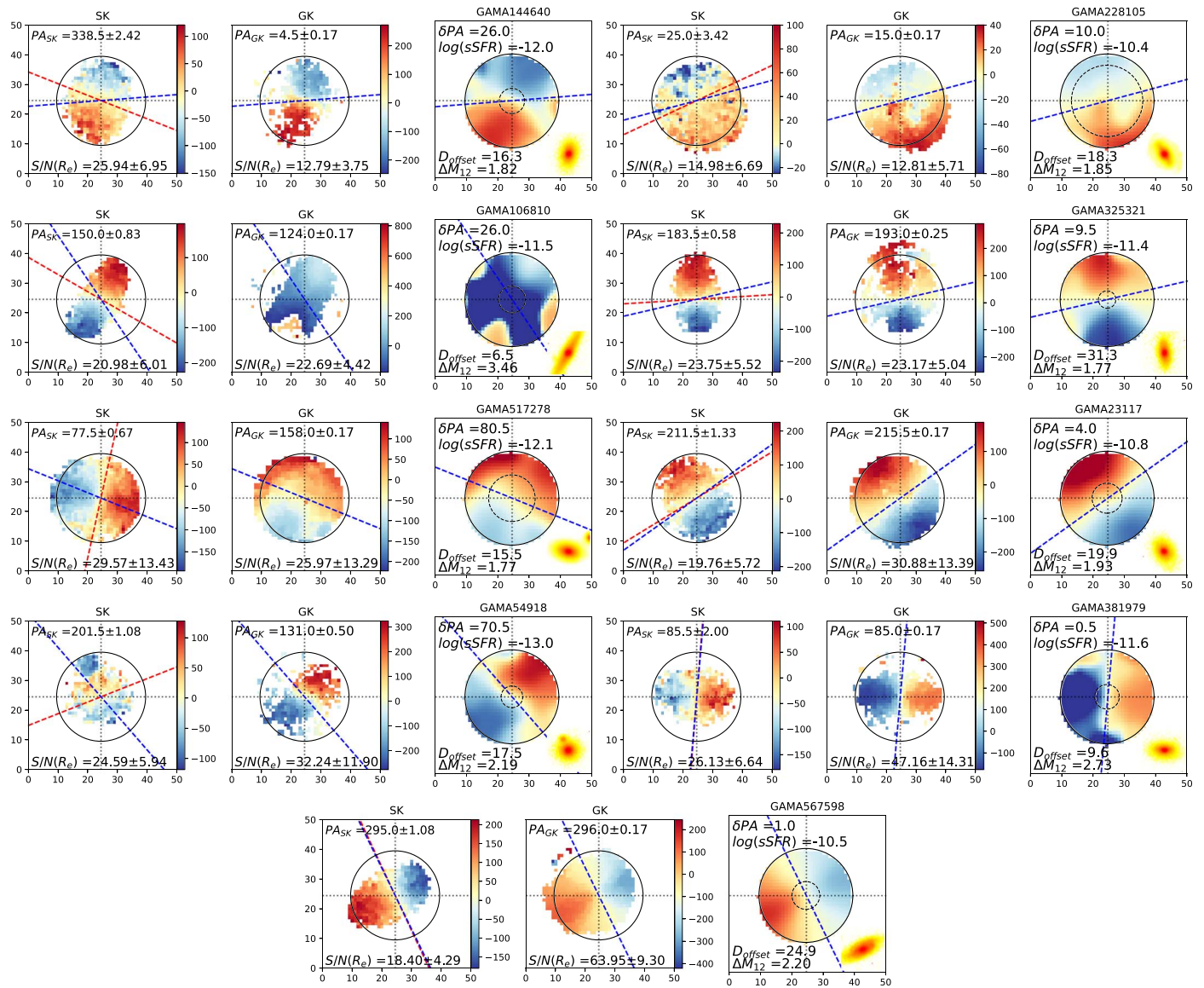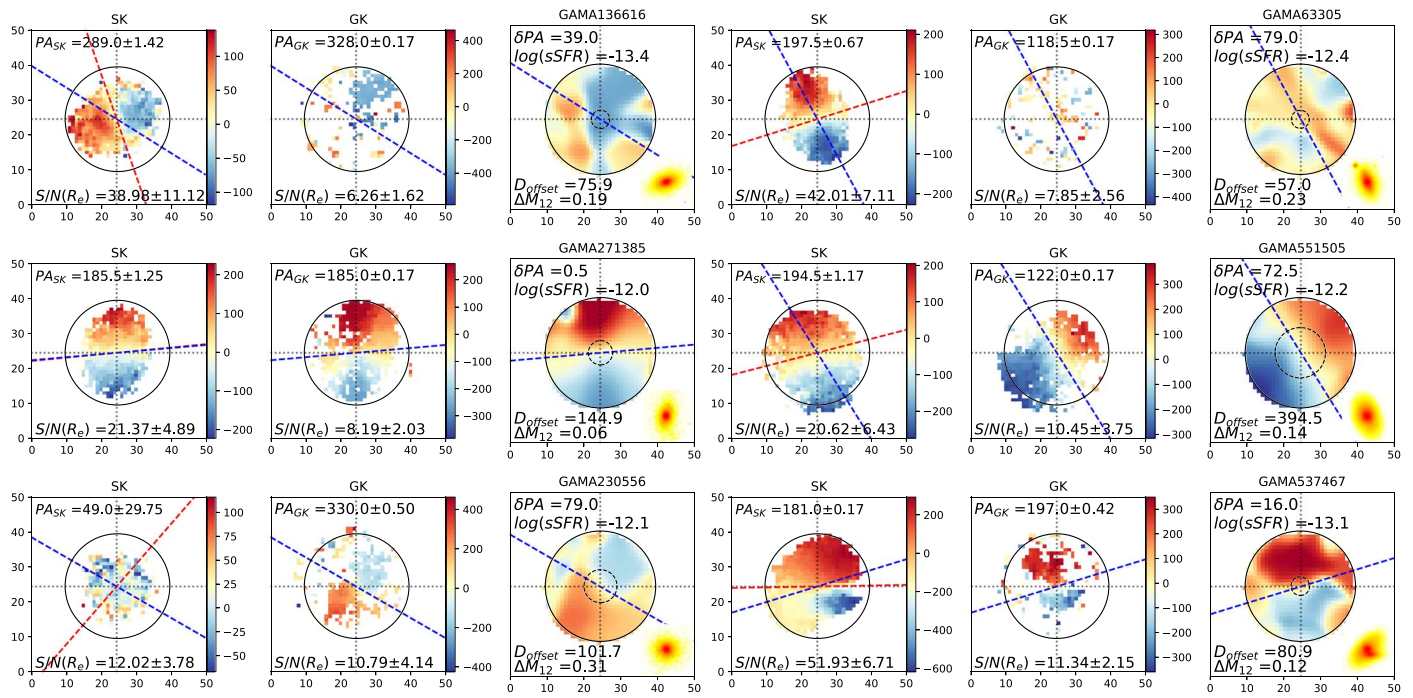
Figure 10. Relaxed group, continued.

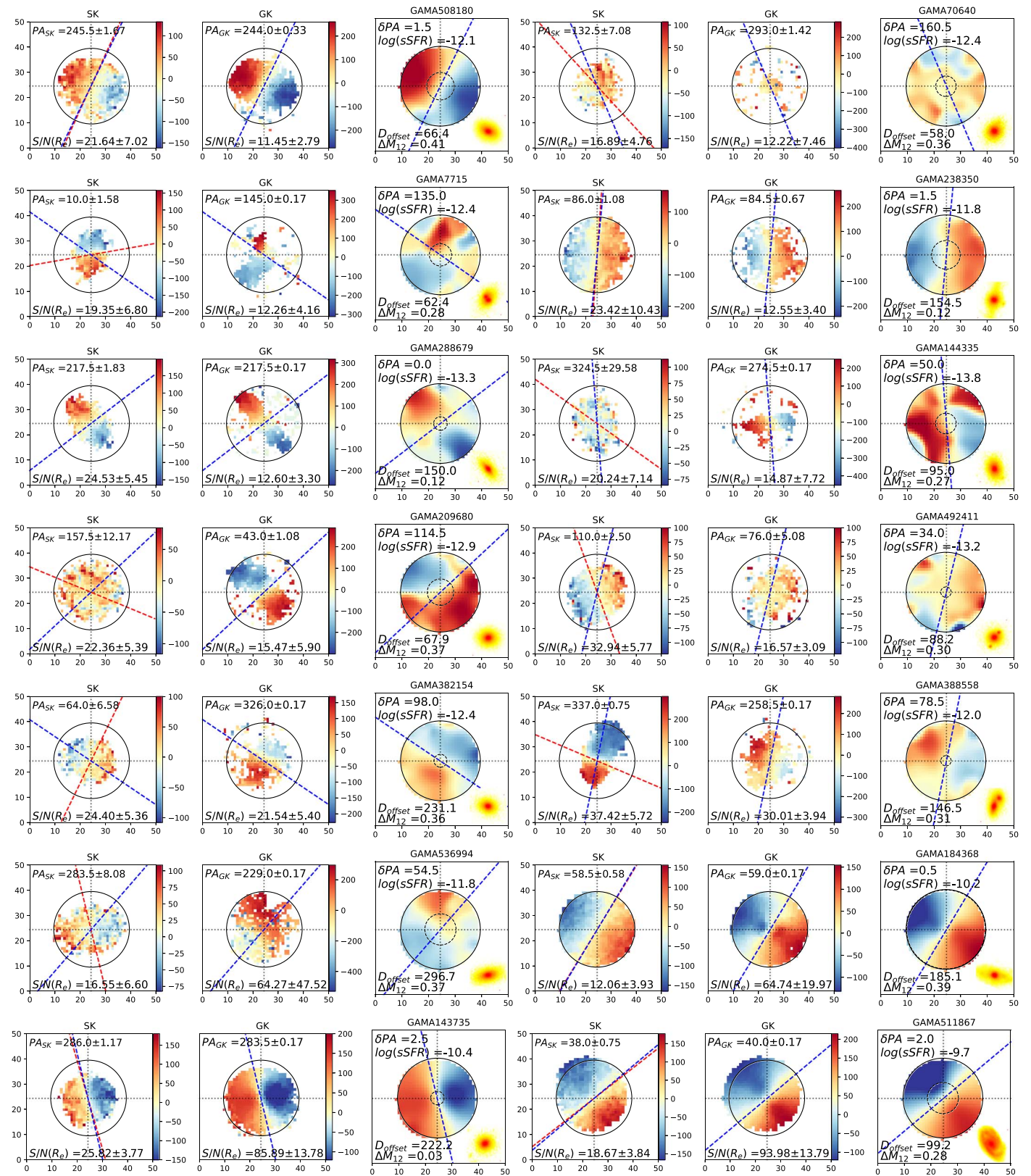**Figure 11.** Same as Figure 9 for unrelaxed groups.

Figure 12. Unrelaxed group, continued.

ORCID iDs

Mojtaba Raouf ⓘ https://orcid.org/0000-0002-1496-3591
Rory Smith ⓘ https://orcid.org/0000-0001-5303-6830
Jesse van de Sande ⓘ https://orcid.org/0000-0003-2552-0021
Julia J. Bryant ⓘ https://orcid.org/0000-0003-1627-9301
Luca Cortese ⓘ https://orcid.org/0000-0002-7422-9823
S. Brough ⓘ https://orcid.org/0000-0002-9796-1363
Ho Seong Hwang ⓘ https://orcid.org/0000-0003-3428-7612
Simon Driver ⓘ https://orcid.org/0000-0001-9491-7327
Jongwan Ko ⓘ https://orcid.org/0000-0002-9434-5936
Jae-Woo Kim ⓘ https://orcid.org/0000-0002-1710-4442
Jihye Shin ⓘ https://orcid.org/0000-0001-5135-1693
Nicholas Scott ⓘ https://orcid.org/0000-0001-8495-8547
Joss Bland-Hawthorn ⓘ https://orcid.org/0000-0001-7516-4016
Matt Owers ⓘ https://orcid.org/0000-0002-2879-1663

References

Allen, J. T., Croom, S. M., Konstantopoulos, I. S., et al. 2015, MNRAS, 446, 1567
Astropy Collaboration, Price-Whelan, A. M., Sipőcz, B. M., et al. 2018, AJ, 156, 123
Astropy Collaboration, Robitaille, T. P., Tollerud, E. J., et al. 2013, A&A, 558, A33
Baldry, I. K., Liske, J., Brown, M. J. I., et al. 2018, MNRAS, 474, 3875
Baldry, I. K., Robotham, A. S. G., Hill, D. T., et al. 2010, MNRAS, 404, 86
Barrera-Ballesteros, J. K., García-Lorenzo, B., Falcón-Barroso, J., et al. 2015, A&A, 582, A21
Bassett, R., Bekki, K., Cortese, L., et al. 2017, MNRAS, 470, 1991
Bland-Hawthorn, J., Bryant, J., Robertson, G., et al. 2011, OExpr, 19, 2649
Brough, S., Forbes, D. A., Kilborn, V. A., & Couch, W. 2006a, MNRAS, 370, 1223
Brough, S., Forbes, D. A., Kilborn, V. A., Couch, W., & Colless, M. 2006b, MNRAS, 369, 1351
Brough, S., van de Sande, J., Owers, M. S., et al. 2017, ApJ, 844, 59
Bryant, J. J., Croom, S. M., van de Sande, J., et al. 2019, MNRAS, 483, 458
Bryant, J. J., Owers, M. S., Robotham, A. S. G., et al. 2015, MNRAS, 447, 2857
Cappellari, M. 2016, ARA&A, 54, 597
Cappellari, M. 2017, MNRAS, 466, 798
Cappellari, M., & Emsellem, E. 2004, PASP, 116, 138
Croom, S. M., Lawrence, J. S., Bland-Hawthorn, J., et al. 2012, MNRAS, 421, 872
Dariush, A. A., Raychaudhury, S., Ponman, T. J., et al. 2010, MNRAS, 405, 1873
Davis, T. A., & Bureau, M. 2016, MNRAS, 457, 272
Driver, S. P., Hill, D. T., Kelvinet, L. S., et al. 2011, MNRAS, 413, 971
Emsellem, E., Cappellari, M., Krajnović, D., et al. 2007, MNRAS, 379, 401
Emsellem, E., Cappellari, M., Krajnović, D., et al. 2011, MNRAS, 414, 888
Farhang, A., Khosroshahi, H. G., Mamon, G. A., Dariush, A. A., & Raouf, M. 2017, ApJ, 840, 58
Fogarty, L. M. R., Scott, N., Owers, M. S., et al. 2014, MNRAS, 443, 485
Green, A. W., Croom, S. M., Scott, N., et al. 2018, MNRAS, 475, 716
Gunn, J. E., & Gott, J. R. 1972, ApJ, 176, 1
Han, S., Smith, R., Choi, H., et al. 2018, ApJ, 866, 78
Hopkins, A. M., Driver, S. P., Brough, S., et al. 2013, MNRAS, 430, 2047
Jin, Y., Chen, Y., Shi, Y., et al. 2016, MNRAS, 463, 913
Jones, L. R., Ponman, T. J., Horton, A., et al. 2003, MNRAS, 343, 627
Kelvin, L. S., Driver, S. P., Robotham, A. S. G., et al. 2012, MNRAS, 421, 1007
Khim, D. J., Yi, S. K., Dubois, Y., et al. 2020a, ApJ, 894, 106
Khim, D. J., Yi, S. K., Pichon, C., et al. 2020b, ApJS, submitted, arXiv:2012.04659
Khosroshahi, H. G., Ponman, T. J., & Jones, L. R. 2006, MNRAS, 372, L68
Khosroshahi, H. G., Raouf, M., Miraghaei, H., et al. 2017, ApJ, 842, 81
Krajnović, D., Bacon, R., Cappellari, M., et al. 2008, MNRAS, 390, 93
Krajnović, D., Cappellari, M., de Zeeuw, P. T., & Copin, Y. 2006, MNRAS, 366, 787
Krajnović, D., Emsellem, E., Cappellari, M., et al. 2011, MNRAS, 414, 2923
Lagos, C. d. P., Padilla, N. D., Davis, T. A., et al. 2015, MNRAS, 448, 1271
Lake, G., & Norman, C. 1983, ApJ, 270, 51
Larson, R. B., Tinsley, B. M., & Caldwell, C. N. 1980, ApJ, 237, 692
Lee, J. C., Hwang, H. S., & Chung, H. 2018, MNRAS, 477, 1567
Mihos, J. C. 2004, in Clusters of Galaxies: Probes of Cosmological Structure and Galaxy Evolution, ed. J. S. Mulchaey et al. (Cambridge: Cambridge Univ. Press), 277
Park, C., & Hwang, H. S. 2009, ApJ, 699, 1595
Ponman, T. J., Allan, D. J., Jones, L. R., Merrifield, M., & MacHardy, I. M. 1994, Natur, 369, 462
Raouf, M., Khosroshahi, H. G., & Dariush, A. 2016, ApJ, 824, 140
Raouf, M., Khosroshahi, H. G., Mamon, G. A., et al. 2018, ApJ, 863, 40
Raouf, M., Khosroshahi, H. G., Ponman, T. J., et al. 2014, MNRAS, 442, 1578
Raouf, M., Shabala, S. S., Croton, D. J., Khosroshahi, H. G., & Bernyk, M. 2017, MNRAS, 471, 658
Raouf, M., Silk, J., Shabala, S. S., et al. 2019, MNRAS, 486, 1509
Raouf, M., Smith, R., Khosroshahi, H. G., et al. 2019, ApJ, 887, 264
Robotham, A., Driver, S. P., Norberg, P., et al. 2010, PASA, 27, 76
Robotham, A. S. G., Norberg, P., Driver, S. P., et al. 2011, MNRAS, 416, 2640
Saremi, E., Javadi, A. T., van Loon, J., et al. 2020, ApJ, 894, 135
Scott, N., van de Sande, J., Croom, S. M., et al. 2018, MNRAS, 481, 2299
Shapiro, K. L., Genzel, R., Schreiber, N. M. F., et al. 2008, ApJ, 682, 231
Sharp, R., Allen, J. T., Fogarty, L. M. R., et al. 2015, MNRAS, 446, 1551
Sharp, R., Saunders, W., Smith, G., et al. 2006, Proc. SPIE, 6269, 62690G
Taylor, E. N., Hopkins, A. M., Baldry, I. K., et al. 2011, MNRAS, 418, 1587
van de Sande, J., Bland-Hawthorn, J., Fogarty, L. M. R., et al. 2017, ApJ, 835, 104
van de Voort, F., Davis, T. A., Kereš, D., et al. 2015, MNRAS, 451, 3269
Zhoolideh Haghighi, M. H., Raouf, M., Khosroshahi, H. G., Farhang, A., & Gozaliasl, G. 2020, ApJ, 904, 36